Frequency Scanning Leaky-Wave Array Antenna with Extended Scanning Range for Millimeter Wave Imaging

Kevin Kipruto Mutai, *Graduate Student Member, IEEE* and Qiang Chen, *Senior Member, IEEE*

***Abstract*—In this letter, we propose a frequency scanning leaky-wave array antenna with a significantly increased scanning range. The proposed structure consists of a pair of rectangular waveguide fed leaky-wave slot array antennas that are designed to achieve focusing in the backward and forward quadrants at 26.5 GHz and 23 GHz respectively. A total scanning range of about 73° is achieved by the structure simply by changing the frequency. The focusing gain between the backward and forward quadrants varies from 23 dBi to 25 dBi with the operation of the two waveguides separated by exploiting the cutoff region of one waveguide, operating with negative phase constant, and the endfire radiation of the other waveguide, operating with a positive phase constant, allowing the use of a single feed for both waveguides.**

***Index Terms*—Frequency scanning antennas (FSAs), leaky-wave antennas (LWAs), slot arrays, near field focusing (NFF)**

I. INTRODUCTION

NEAR field focusing (NFF) antennas, moreso of the one dimensional leaky-wave antenna (LWA) variety, have drawn attention owing to their relatively portable physical profiles and ease of electronically scanning through one spatial dimension simply by changing the frequency [1] – [7]. Owing to these advantages, the applicability of such structures has been explored in millimeter wave imaging [8], [9] to reduce the fabrication costs involved in contemporary imaging systems where arrays of sensors [10] – [12] have been reduced to a pair of near-field focusing leaky-wave antennas. The requirement for a large dielectric lens or reflectors used in other systems [13], [14] is also largely eliminated allowing for less bulky designs.

Despite these advantages, a challenge present in current frequency scanning NFF LWA designs is the limitation of the available scanning range to the forward quadrant [4] – [6] which is an inherent characteristic of uniform LWAs. To overcome this limitation, a periodic approach can be used [1], [9] at the expense of an increased scanning range. A conformal approach may also be used [2], [3] which may allow for an increased scanning range but at the expense of a compact physical profile.

This paragraph of the first footnote will contain the date on which you submitted your paper for review, which is populated by IEEE. This work was supported in part by the Program on Open Innovation Platform with Enterprises, Research Institute and Academia, Japan Science and Technology Agency (OPERA, JST) under Grant JPMJOP1852. (*Corresponding author: Kevin Kipruto Mutai*).

The authors are with the Department of Communications Engineering, Graduate School of Engineering, Tohoku University, 6-6-05 Aramaki Aza Aoba, Aoba-ku, Sendai, Miyagi, 980-8579, Japan (mutai-k@ecei.tohoku.ac.jp; chenq@ecei.tohoku.ac.jp).

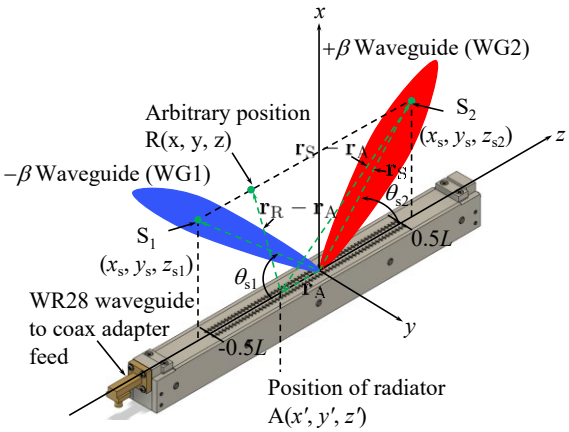

Fig. 1. Concept of proposed frequency scanning structure.

To address these challenges, we put forward a compact rectangular waveguide-based frequency scanning LWA capable of NFF. The novelty of the proposed approach lies in the focusing effect being achieved in both the forward and backward quadrants using a single-port excitation thereby theoretically effectively doubling the available scanning range compared to contemporary structures of a similar nature [4] – [6]. This is achieved by appropriate tapering of the phase constant (β) of the traveling wave in two slitted waveguides (See Fig. 1) capable of a negative β (WG1) [15] and positive β (WG2) [16] which allows for the use of a single feed located at one end. The use of single-port excitation allows for a relatively simple, cheap and compact feeding mechanism compared to a dual-port approach which would require double the RF chain components.

II. DESIGN AND CHARACTERIZATION OF PROPOSED STRUCTURE

A. Design of the Proposed Structure

To achieve the desired focusing effect at the target focusing positions of $S_1(x_s = 195$ mm, $y_s = 0$ mm, $z_{s1} = -150$ mm) and $S_2(x_s = 195$ mm, $y_s = 0$ mm, $z_{s2} = 150$ mm) for WG1 and WG2 respectively, the phase constant distribution ($\beta_z(z')$) of the travelling wave along the longitudinal direction (z direction) of both WG1 and WG2 needs to be appropriately tapered. As such, the required $\beta_n(z')$ can be derived from the phase

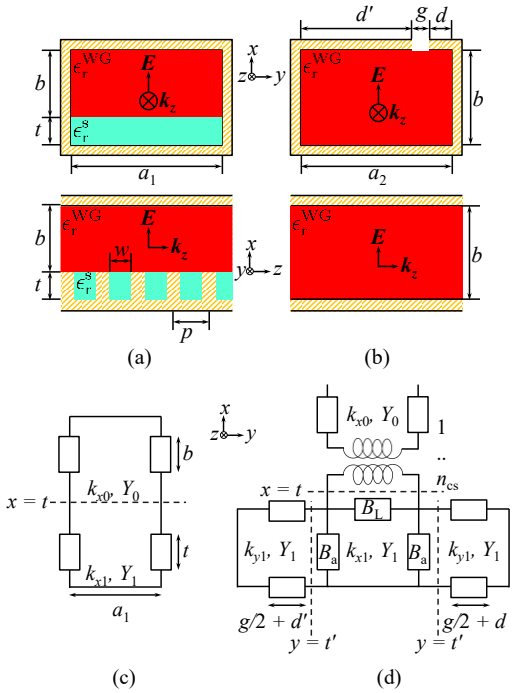

Fig. 2. Transverse and longitudinal views of (a) WG1 and (b) WG2. Transverse equivalent networks of (c) WG1 and (d) WG2.

differences in the near field between an arbitrary position in the *xz*-plane above the position of each radiator, in the range $-0.5L \le z' \le 0.5L$, and the focusing position $S_n(x_s, y_s, z_{sn})$ where n can be 1 or 2 depending on the waveguide under consideration. The $\beta_n(z')$ for WG1 and WG2 can therefore be expressed as [17]

$$\beta_1(z') = -k_0 \frac{z_s - z'}{\sqrt{(z_s - z')^2 - x_s^2}} \tag{1}$$

and

$$\beta_2(z') = k_0 \frac{z_s - z'}{\sqrt{(z_s - z')^2 - x_s^2}} \tag{2}$$

respectively. Note that the same positive value of z_s can be used in both (1) and (2) as the negative sign for focusing in the backward quadrant in the case of WG1 is introduced into (2) by virtue of $-\beta_1(z')$.

Having (1) and (2), the next step is to then actualize the physical tapering in WG1 and WG2. To accomplish this, the equivalent networks of both waveguides are used as presented in [15] and [16] to derive a relationship between the β_z and some physical parameter we wish to taper to achieve (1) and (2). For WG1, the characteristic equation for the dominant TE mode from (32) to (34) in [15] is

$$Y_{\text{tot, 1}} = Y_{0,1} + Y_{1,1} = 0 \tag{3}$$

where

$$Y_{0,1} = \frac{k_{x0,1}}{\omega\mu_{0,1}} \left[\frac{wa_1}{2p} \frac{\gamma^2}{k_{x1}} \left(\frac{\sin(k_{z1}\frac{w}{2})}{k_{z1}\frac{w}{2}} \right)^2 \right] j\cot(k_{x0,1}b) \tag{4}$$

$$Y_{1,1} = \frac{k_{x1,1}}{\omega\mu_0} \cot(k_{x1,1}t) \tag{5}$$

in which

$$k_{x0,1} = \sqrt{\epsilon_r^{WG} k_0^2 - (k_{z1}^2 + \left(\frac{\pi}{a}\right)^2)} \tag{6}$$

$$\gamma = \sqrt{\epsilon_r^{WG} k_0^2 - \left(\frac{\pi}{a}\right)^2} \tag{7}$$

$$k_{x1,1} = \sqrt{\epsilon_r^{s} k_0^2 - \left(\frac{\pi}{a}\right)^2}. \tag{8}$$

Equation (4) is the short-circuited input admittance of the corrugation in Fig. 2(a) with length t whereas (5) is a similar value for the waveguide section viewed upwards from the reference plane set at $x = t$ in Fig. 2(c) with length b. The periodicity of the corrugations are included in the term in square brackets in (5). For WG2 represented in Fig. 2(b) and (d), the equation describing the network is [16]

$$Y_{\text{tot},2} = Y_{0,2} + Y_{1,2} = 0 \tag{9}$$

where

$$Y_{0,2} = \frac{k_{x1,2}}{\omega\mu_0} \frac{1}{n_{cs}^2} \tag{10}$$

$$Y_{1,2} = jB_L + \frac{1}{\frac{1}{jB_a + Y_R} + \frac{1}{jB_a + Y_L}} \tag{11}$$

in which the variables in (10) and (11) are as outlined in equations (4) to (7) and (9) in [16].

In the proposed structure, we wish to physically achieve (1) and (2) by tapering the waveguide broad wall heights, a_n. This physical variable was selected owing to the relative manufacturing ease and anticipated fine periodicity of the $\beta_n(z')$ which would allow maximum possible resolution compared to other physical variables. To separate the operation of the two waveguides and avoid interference between the radiated electric fields from WG1 and WG2, WG1 is air-filled ($\varepsilon_r^{WG} = 1$) whereas WG2 is dielectric filled ($\varepsilon_r^{WG} = 2.1$) thereby lowering the cutoff frequency, and consequently the operating frequency range, of WG2.

To derive the relationship between a_n and β_n, a_1 was changed in (6) to (8) in the range 5 mm $\le a_1 \le$ 5.625 mm in 0.125 mm increments for WG1 with b = 2.5 mm, t = 2.5 mm, p = 1.5 mm, w = 1.175 mm and $\varepsilon_r^S = 2.75$. Similarly, a_2 was varied in the range 5 mm $\le a_2 \le$ 6 mm with g = 1 mm in 0.25 mm increments for WG2 as indicated in Fig. 3 (a) with $\varepsilon_r^{WG} = 2.1$. These equations with the different values of a_n were then substituted into (3) to (5) and (9) to (11) and solved numerically for the normalized wavenumbers in the longitudinal direction, k_{z1} and k_{z2} in WG1 and WG2 respectively. To solve for k_{z1}, the limits of the solution were set to be $0 \le \beta_{z1} \le 1$ for the real part with $\alpha_{z1} = 0$ for the imaginary part. This is because the closed waveguide model is used in this case. However, because the $-\beta$ exists in the cutoff region, the introduction of a slit would have no influence on the $-\beta$ [18] thereby enabling the use of the closed waveguide model. In the case of WG2, the limits were set as $0 \le \beta_{z2} \le 1$

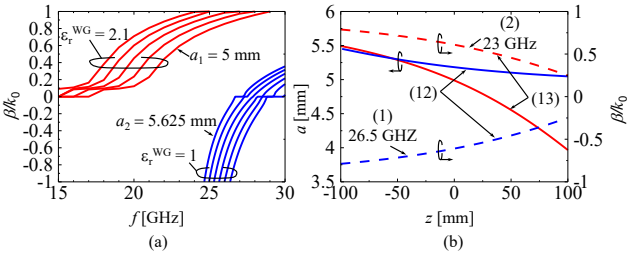

Fig. 3. Normalized (a) phase constant of WG1 ($\varepsilon_r^{WG} = 1$) and WG2 ($\varepsilon_r^{WG} = 2.1$). Required (b) normalized phase constant distribution ($\beta(z')$) to focus on S1 and S2 and corresponding $a(z')$.

and $0 \leq \alpha_{z2} \leq 1$.

The design frequencies were then selected as 26.5 GHz and 23 GHz for WG1 and WG2 respectively with the understanding that with these two values, the operation of WG1 and WG2 would be separated. The operation of WG2 would be in the cutoff region of WG1 and the positive β range of WG1 would be in the end fire operation of WG2. With this in mind, the relationship between a_n and normalized β_n at the design frequencies was then derived by interpolation and was found to be

$$a_1(z') = 0.7554\left(\frac{\beta_1(z')}{k_0}\right) + 5.6432 \qquad (12)$$

$$a_2(z') = 2.8289\left(\frac{\beta_2(z')}{k_0}\right) + 3.2634 \qquad (13)$$

for WG1 and WG2. The results of (12) and (13) are plotted in Fig. 3 for L = 200 mm with (1) and (2) substituted in and, interestingly, both (12) and (13) are in the same direction which hints at the possibility of achieving a similar backwards to forwards quadrant scanning NFF structure based on a single waveguide.

A prototype with (12) and (13) was fabricated and is indicated in Fig. 4. To divide the input power between the two waveguides, a sharply tapered divider of 2 mm width was used to prevent reflections back to the WR28 waveguide to co-ax adapter used as the feed. The dielectric fillings used within the corrugations in WG1 and the dielectric filling in WG2 were fabricated by 3D printing using polylactic acid (PLA) material with dielectric constant of ε_r^D = 2.75 and as such the loss tangent of PLA was considered in the derivation of (12) and (13) as tan δ = 0.01. The ε_r^{WG} = 2.1 was accomplished by setting the filling rate, $\zeta = (\varepsilon_r^{WG} - 1)/(\varepsilon_r^D - 1) = 0.63$.

The broad wall height at the section interfaced with the feed was set to be a_{f1} = 7.112 mm to match the feed dimensions. The a_{f1} was then flared into a_{f2} = 8 mm which was then divided into a_t = 9 mm to allow the propagation in the required operating frequency range of 21.5 GHz to 30.5 GHz. A matching layer section was added to WG2 to minimize reflections to the feed with t_{ML} = 1.5 mm and l_{ML} = 3.5 mm which were decided upon by following the guidelines outlined in [19] at 23 GHz for ε_r^{WG} = 2.1. To allow the leakage of the travelling wave within the WG1 and WG2, the longitudinal slit was placed offset from the center with d = 1.5 mm in both WG1 and WG2 and the taper of a_n being effected by d'. In addition to the longitudinal slit with g = 1 for both structures,

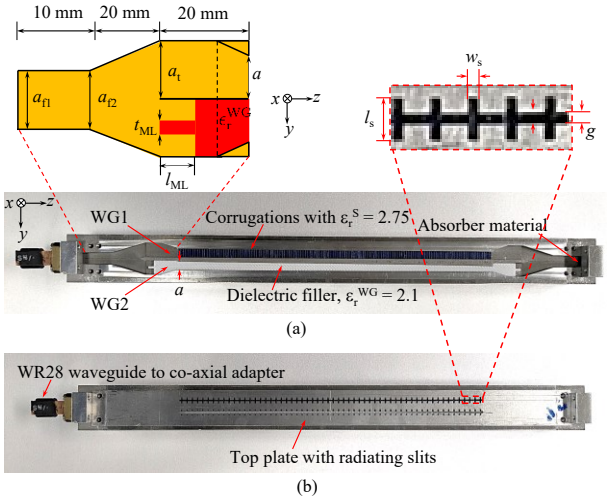

Fig. 4. Fabricated prototype (a) without the top plate installed and (b) with the top plate installed.

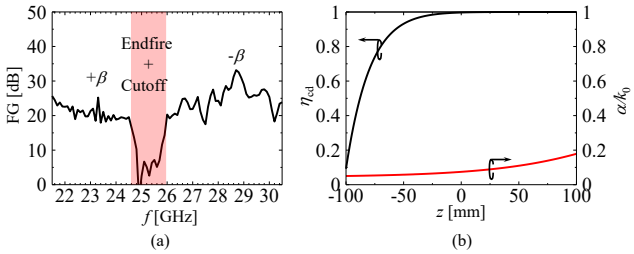

Fig. 5. The (a) focusing gain (FG) of the proposed structure and (b) the attenuation constant distribution ($a(z')$) and corresponding radiation efficiency distribution ($\eta_{cd}(z')$).

shorter transverse slots were introduced along the length of the longitudinal slits with length l_s = 4 mm, width w_s = 1 mm and with a periodicity of 3.5 mm to allow the radiation of not only the y component of the electric field from the longitudinal slit, but also the z-component thereby achieving a 45˚shifted linear polarization along the yz-plane, which may be useful for imaging applications to allow the detection and subsequent imaging of arbitrarily oriented objects by polarization diversity without having to move the antennas physically.

B. Focusing Gain, Efficiency, Resolution and Scanning Range

A metric that can be used to characterize NFF structures is the focusing gain (FG) which is defined as the ratio of the power density of the NFF structure to the power density of the corresponding untapered structure in the far field [20] - [22]. As such, the FG of the proposed structure was calculated from full-wave simulation results and is shown in Fig. 5(a) where the average FG for WG1 was found to be 25 dBi whereas that of WG2 was found to be 23 dBi indicating a drop of 2 dB between the backward to forward quadrant. This drop may be partly attributed to the design frequency of WG2, from Fig. 3(a), being close to the surface wave operation ($\beta_z \geq k_0$) for the given values of a_2 which may lead to a drop in the radiated electric field at the focusing spot as f is increased.

To evaluate the radiation efficiency, η_{cd}, of the proposed NFF structure, the following expression was used

$$\eta_{cd}(z') = 1 - e^{-2\int_{-0.5L}^{z'} \alpha(z')dz'} \qquad (14)$$

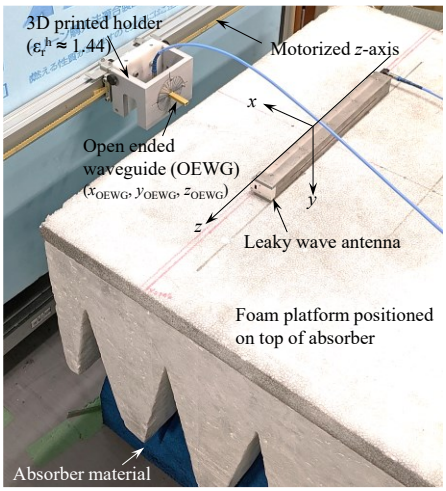

Fig. 6. Experiment setup to measure radiated electric field distribution from proposed structure.

where the $\alpha(z')$ for WG2 was extracted using the equivalent network (as $\beta_1(z')$ exists in the cutoff region of WG1) and is indicated in Fig. 5(b). This $\alpha(z')$ was plugged into (14) and the average η_{cd} was found to be 0.9043 at 23 GHz.

To evaluate the illumination efficiency $\eta_i = \eta_s \eta_p \eta_t$ where η_s was found to be 1 by setting $z' = 0.5L$ in (14). The phase and taper efficiency, $\eta_p \eta_t$, were then found by calculating the difference between the peak directivity in the analytical case (with continuous phase tapering) with the peak directivity extracted from the simulation and the difference (in dB) between the two values being the phase and taper loss. The near field directivity, D, was defined by [23]

$$\mathrm{D} = \frac{x_s}{\mathrm{FWHM}} \tag{15}$$

where FWHM is the full width at half maximum. The average η_i between WG1 and WG2 was found to be 0.6118.

The fabricated prototype was then measured using the experiment setup indicated in Fig. 6 where the OEWG was moved along the z-axis at $x = x_s$ with $y = y_s = 0$ and the transmission coefficient between the OEWG and the LWA was measured for each position z and the results indicated in Fig. 7(a) and (c). To prevent reflections from the OEWG holder, it was 3D printed using $\zeta = 0.25$ to achieve a dielectric constant of $\varepsilon_r^h \approx 1.44$. The average mismatch efficiency, η_r, was then found to be 0.8726 from the measured return loss in Fig. 7(a) for the operating frequency range. The overall average efficiency of the proposed structure was then found to be 0.4844.

The resolution of the proposed structure along the z direction, as observed from the 3dB width in measurement results in Fig. 7(c), seems to average about 33 mm for WG1 and about 32 mm for WG2 which indicates stable resolution in both the backward and forward quadrants. From Fig. 7(b), the maximum simulated scanning range was found to be about 89° taking -177 mm ≤ z ≤ 200 mm with x = 195 mm. However, in the measured case, the scanning range was found to be about 73° taking -125 mm ≤ z ≤ 160 mm which, though short of the expected 90°, is significantly greater than the 6° and 38° in [2] and [3] respectively or the theoretically achievable maximum

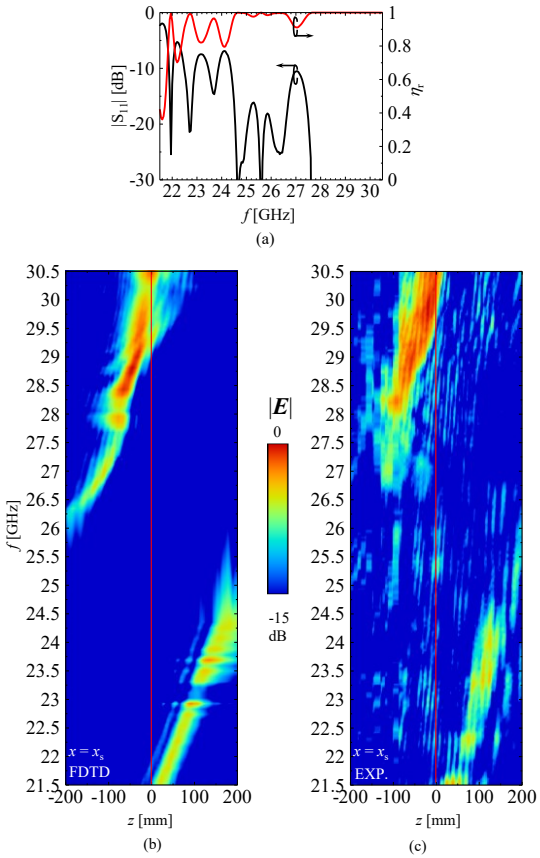

Fig. 7. Return loss (a) of proposed structure and corresponding mismatch efficiency ($\eta_r(f)$). Simulated radiated electric field along the z-direction (b) and the (c) measured electric field distribution.

of 45° in [4] – [6] or the 23° achieved in [9] thereby validating the usefulness of the proposed structure.

Despite the extended scanning range achieved using the proposed structure, a challenge apparent from the measurement results is the drop in the radiated electric field at some frequencies, especially in the low frequency region. This is attributed to the cutoff effect appearing at these frequencies owing to the use of WR28 coax to waveguide adapter which is not designed to perform optimally at the affected frequencies. As such, future designs would take this into account to further optimize the feed and improve the achieved performance.

III. Conclusion

In this letter, a frequency scanning NFF LWA structure with a significantly increased scanning range making use of a single-port excitation dual-waveguide design was proposed and the stated goal of a significantly increased scanning range was verified by simulation and experimentally. The prototype was shown to achieve a theoretical scanning range of about 89° and a measured scanning range of about 73° with the difference being attributed to a sub-optimal feed design. Apart from the optimization of the feed, a possible future direction would be to reduce the dual-waveguide design to a single waveguide structure thereby reducing the physical profile even further.

REFERENCES

[1] T. Okuyama, Y. Monnai and H. Shinoda, "20-GHz Focusing Antennas Based on Corrugated Waveguide Scattering," *IEEE Antennas Wireless Propag. Lett.*, vol. 12, pp. 1284-1286, 2013.

[2] I. Ohtera, "Focusing properties of a microwave radiator utilizing a slotted rectangular waveguide," *IEEE Trans. Antennas Propag*., vol. 38, no. 1, pp. 121-124, Jan. 1990.

[3] Y. F. Wu and Y. J. Cheng, "Proactive Conformal Antenna Array for Near-Field Beam Focusing and Steering Based on Curved Substrate Integrated Waveguide," *IEEE Trans. Antennas Propag*., vol. 67, no. 4, pp. 2354-2363, April 2019.

[4] J. L. Gomez-Tornero, F. Quesada-Pereira, A. Alvarez-Melcon, G. Goussetis, A. R. Weily and Y. J. Guo, "Frequency Steerable Two Dimensional Focusing Using Rectilinear Leaky-Wave Lenses," *IEEE Trans. Antennas Propag*., vol. 59, no. 2, pp. 407-415, Feb. 2011.

[5] A. J. Martínez-Ros, J. L. Gómez-Tornero, F. J. Clemente-Fernández and J. Monzó-Cabrera, "Microwave Near-Field Focusing Properties of Width-Tapered Microstrip Leaky-Wave Antenna," *IEEE Trans. Antennas Propag*., vol. 61, no. 6, pp. 2981-2990, June 2013.

[6] T. Hashimoto, H. Sato, and Qiang Chen, "Near-field leaky-wave focusing antenna with inhomogeneous rectangular waveguide," *IEICE Commun. Exp.*, vol.9, vo.6, pp. 1-6, June, 2020.

[7] K. K. Mutai, H. Sato and Q. Chen, "Near Field Leaky Wave Focusing Antenna with Tapered Dielectric Constant Distribution," *IEEE Antennas Wireless Propag. Lett.*, doi: 10.1109/LAWP.2023.3236644.

[8] K. K. Mutai, H. Sato and Q. Chen, "Active Millimeter Wave Imaging Using Leaky-Wave Focusing Antenna," *IEEE Trans. Antennas Propag*., vol. 70, no. 5, pp. 3789-3798, May 2022.

[9] S. Li and S. Wu, "Low-Cost Millimeter Wave Frequency Scanning Based Synthesis Aperture Imaging System for Concealed Weapon Detection," *IEEE Trans. Microw. Theory Techn.*, vol. 70, no. 7, pp. 3688-3699, July 2022.

[10] D. M. Sheen, D. L. McMakin, and T. E. Hall, "Three-dimensional millimeter-wave imaging for concealed weapon detection," *IEEE Trans. Microw. Theory Techn.*, vol. 49, no. 9, pp. 1581–1592, Sep. 2001.

[11] S. Vakalis, L. Gong, Y. He, J. Papapolymerou, and J. A. Nanzer, "Experimental demonstration and calibration of a 16-element active incoherent millimeter-wave imaging array," *IEEE Trans. Microw. Theory Techn.*, vol. 68, no. 9, pp. 3804–3813, Sep. 2020.

[12] W. Fang, P. Fei, F. Nian, Y. Yang, and K. Feng, "Ka-band dielectric waveguide antenna array for millimeter wave active imaging system," *J. Infrared, Millim., Terahertz Waves*, vol. 35, no. 11, pp. 962–973, Nov. 2014.

[13] H. Sato, K.Sawaya, K. Mizuno, J. Uemura, M. Takeda, J. Takahashi, K. Yamada, K. Morichika, T. Hasegawa, H. Hirai, H. Niikura, T. Matsuzaki, S. Kato and J. Nakada, "Passive millimeter-wave imaging for security and safety applications", *Proc. SPIE*, vol. 7671, 2010.

[14] D. A. Andrews, S. W. Harmer, N. J. Bowring, N. D. Rezgui, and M. J. Southgate, "Active millimeter wave sensor for standoff concealed threat detection," *IEEE Sensors J.*, vol. 13, no. 12, pp. 4948–4954, Dec. 2013.

[15] I. A. Eshrah, A. A. Kishk, A. B. Yakovlev and A. W. Glisson, "Spectral analysis of left-handed rectangular waveguides with dielectric-filled corrugations," *IEEE Trans. Antennas Propag*., vol. 53, no. 11, pp. 3673-3683, Nov. 2005.

[16] F. Frezza, P. Lampariello, H. Shigesawa, M. Tsuji and A. A. Oliner, "A versatile leaky-wave antenna based on stub-loaded rectangular waveguide .II. Effects of flanges and finite stub length," *IEEE Trans. Antennas Propag*., vol. 46, no. 7, pp. 1042-1046, July 1998.

[17] P. Burghignoli, F. Frezza, A. Galli and G. Schettini, "Synthesis of broadbeam patterns through leaky-wave antennas with rectilinear geometry," *IEEE Antennas Wireless Propag. Lett.*, vol. 2, pp. 136-139, 2003.

[18] M. Navarro-Tapia, J. Esteban and C. Camacho-Penalosa, "On the Actual Possibilities of Applying the Composite Right/Left-Handed Waveguide Technology to Slot Array Antennas," *IEEE Trans. Antennas Propag*., vol. 60, no. 5, pp. 2183-2193, May 2012.

[19] R. Collin and J. Brown, "The design of quarter-wave matching layers for dielectric surfaces," *Proc. IEE Part C: Monographs*, vol. 103, pp. 153–158, 1956.

[20] R. Hansen, "Focal region characteristics of focused array antennas," *IEEE Trans. Antennas Propag*., vol. 33, no. 12, pp. 1328-1337, December 1985.

[21] A. Buffi, P. Nepa and G. Manara, "Design Criteria for Near-Field-Focused Planar Arrays," *IEEE Antennas and Propagation Magazine*, vol. 54, no. 1, pp. 40-50, Feb. 2012.

[22] P. Nepa and A. Buffi, "Near-Field-Focused Microwave Antennas: Near-field shaping and implementation," *IEEE Antennas Propag. Mag.*, vol. 59, no. 3, pp. 42-53, June 2017.

[23] K. A. Thackston and D. F. Sievenpiper, "Limits of Near-Field Directivity for a Wire Array," *IEEE Magnetics Letters*, vol. 9, pp. 1-4, 2018.